A Multi-Component Nanocomposite Screen-Printed Ink with Non-Linear Touch Sensitive Electrical Conductivity

Alexander J Webb[1*], Marek Szablewski[1], David Bloor[1,2], Del Atkinson[1], Adam Graham [2], Paul Laughlin[2] and David Lussey [2].

[1]Department of Physics,
Durham University, South Road, Durham, DH1 3LE, UK
[2]Peratech Ltd.,
Old Repeater Station, 851 Gatherley Road, Brompton on Swale, DL10 7JH, UK
*Corresponding author email: a.j.webb@durham.ac.uk
Phone: 01913343529

Short title: **Nanocomposite Printable Ink**

Classification (PACS): 62.23.Pq, 79.70.+q, 73.63.-b, 81.40.Lm, 81.40.Rs

Abstract. Printable electronics is an innovative area of technology with great commercial potential. Here, a screen-printed functional ink, comprising a combination of semi-conductive acicular particles, electrically insulating nanoparticles and a base polymer ink, is described that exhibits pronounced pressure sensitive electrical properties for applications in sensing and touch sensitive surfaces. The combination of these components in the as-printed ink affect a complex structure and a large and reproducible touch pressure sensitive resistance range. In contrast to some composite systems, the resistance changes occur down to applied pressures of 13 Pa. Current-Voltage measurements at fixed pressures show monotonic non-linear behaviour, which becomes more ohmic at higher pressures and in all cases shows some hysteresis. The physical basis for conduction, particularly in the low pressure regime, can be described in terms of field assisted quantum mechanical tunnelling.

1. Introduction

Printable electronics is now an established area of technology with significant commercial potential in a wide range of application sectors that includes photovoltaics, super-capacitors and RFID.[1-3] The development of technologies with electronic functionality that can be mass produced by printing processes has the potential to provide technical benefits, including lighter weight components, and can lead to significant cost benefits from the manufacturing process.

A wide range of materials and functionalities are currently under investigation for printable manufacture, from simple electrically conductive tracks,[4] to flexible FETs.[5] An area of growing applications importance is touch sensitive components and surfaces for switching and position sensing. In its simplest form touch sensitivity requires some contact-sensitive switching capability. The addition of pressure sensitivity adds a third dimension to conventional two-dimensional touch surface interfaces, providing an additional input parameter based upon the applied force in addition to the surface location.

Functional force and location sensing touch pad technology based upon contact-resistance produced by printing has been demonstrated elsewhere.[6,7] However, this approach involved additional patterning, through lithographic and printing methods, on top of a resistive layer or with the addition of features to create regular structures that were needed to create the pressure and location sensing capacity.[6,7] An alternate approach is to develop an ink that is insulating when no pressure is applied, but has an intrinsic pressure sensitive electrical response, allowing direct printing of pressure sensitive components without the need for additional patterning and structures.

In bulk form pressure sensitive electrically conducting switching composites have been a focus of research for over 50 years.[8] The first conductive composites were composed of metal or other conductive filler powders, such as nickel or carbon black, dispersed within insulating elastomers, such as rubber.[9,10] The variation of conductivity behaviour of such composites with filler loading has been described using percolation and effective medium theories, whereby the conductivity of the composite takes a value close to that of the bulk insulating matrix at low filler loading, and rises dramatically at the percolation threshold, a critical filler loading where direct electrical connections form between filler particles throughout the insulating matrix.[11] Such carbon black based conducting composites have been developed as inks for pressure sensing.[12] However, as the composite is loaded above the percolation threshold printed films have a finite start resistance and exhibit an inverse relationship between the starting resistance and pressure sensitivity of the resistive behaviour. Other research has shifted towards composites with filler particles of varying geometries and a wider range of insulating matrices.[13-15]

For printing applications the challenge is to develop composite materials with appropriate pressure sensitive electrical behaviour coupled with the structural requirements needed for preparation as inks that can be printed using conventional print technologies. Such composite materials are not uncommon, having been a focus or research for use as conductive tracks and electrodes, chemical sensors and thin film transistors, and often comprise nanoscale conductive filler particles dispersed in a flowing polymer.[16-20] The progression to nanoscaled filler particles has enabled the use of ink-jet printing for many of these composite materials; larger particles tend to clog the printer nozzles. This work presents a description of the functional behaviour and physical structure of a new type of screen-printed composite ink with electrical properties that are highly sensitive to applied force. Investigation of the I-V behaviour at constant pressure provides some insight into the physical mechanisms that may be responsible for the pressure sensitive electrical behaviour.

2. Ink Production and Experimental Procedure

2.1. Ink Electrical Test Devices

The pressure sensitive ink comprises a combination of acicular, wide band-gap semi-conductive titanium dioxide needles (typically 3 μm x 100 nm) with a more electrically conductive antimony doped tin oxide semi-conductive surface coating and approximately spherical, wide band-gap (essentially

electrically insulating) titanium dioxide nanoparticles (typically with a diameter of ~200 nm), dispersed in an electrically insulating flowing polymer ink, such as an epoxy or polyvinyl resin.[21] The nanoparticles have a surface coating of an organic dispersant, which aids dispersion in the polymeric base ink ensuring a more uniform distribution between the acicular particles. The dispersant used is a typical, commercially available surfactant, such as Triton X. The conductive acicular particles and insulating nanoparticles are added to the polymer ink and are mixed until a homogeneous particulate suspension is obtained. Pressure sensors are prepared by screen printing. The structure of the devices is described below. Following printing, the ink is dried for 30 minutes at 90 °C, evaporating the solvents, which facilitates cross-linking of the polymeric component of the ink.[21]

Electrical test device structures were produced by screen-printing successive layers of material onto two flexible polyethylene terephthalate (PET) substrates, using a manual load semi-automatic flat bed screen print machine, capable of printing up to A3 sized images with a tolerance of one micrometre across the thickness of a printed area. The lower element was fabricated by first printing a silver conducting track and carbon contact pad on the PET followed by a layer of the pressure sensitive ink ~10 μm thick. The upper element comprised a carbon contact pad and connecting conductive silver track printed on a separate PET substrate. This was placed in registry with the lower element to form the test structure. Tests structures were made 5 mm in diameter. Figure 1 (a) shows a schematic cross section of the multilayered structure and figure 1 (b) shows a photograph of a test device.

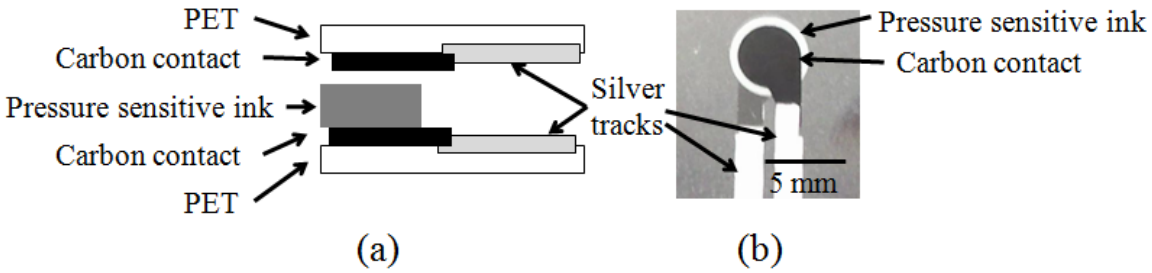

Figure 1. (a) Schematic cross-section of printed structure for the pressure sensitive test device (not to scale) and (b) Photograph showing top view of a printed test device. The force probe is applied to the centre of the printed disk.

2.2. Structural Analysis

Structural analysis of the as-printed ink surfaces was undertaken with a Hitachi SU70 Analytical Scanning Electron Microscope.

2.3. Mechanical Testing and Electrical Characterization Mechanical force tests

Test devices were subject to mechanical and electrical characterization in the form of experiments to determine the sensitivity of the electrical resistance to compressive stress and current-voltage sweeps at static compressions. These were performed using a Lloyd LRX test station using a Tricor Rubber Tip Model 933A force probe, conforming to ASTM standard F1578, designed to replicate the response of finger pressure. In addition to pressure sensitive resistance measurements, current-voltage (I-V) measurements were made under constant load with a computer controlled Keithley 2420 sourcemeter and a custom compression rig manufactured from a micrometer spindle mechanism. The voltage across the sample was ramped up to 10 V in 0.1 V steps over 100 seconds and decreased to 0 V at the same rate. The whole process was then repeated for 10 cycles. Sensors made without the novel ink (just carbon and silver) were also tested to ensure an ohmic response to voltage under all compressions.

3. Results and Discussion

The inks analyzed in this study were made with filler particle concentration and size to optimize properties for touch and location sensing and the results presented here are typical of all samples used in this research.

Both large area and detailed structure of the as-printed ink surface, observed by high-resolution scanning electron microscope imaging, are shown in figure 2. The acicular filler particles are widely dispersed across the surface, although they tend to form clusters comprising a few particles in many places. The acicular particles are randomly oriented both on the surface and into the ink layer. This structuring is important for the pressure sensitive conduction mechanisms. In contrast, the near spherical nanoparticles are more uniformly dispersed. The spherical particles prevent the acicular particles aligning and aggregating with one another into an ordered liquid crystal like structure. The spherical particles probably also play a role in preventing preferential alignment of the acicular particles during screen printing**.** Also of note are voids in the printed ink which contribute to the materials compressibility.

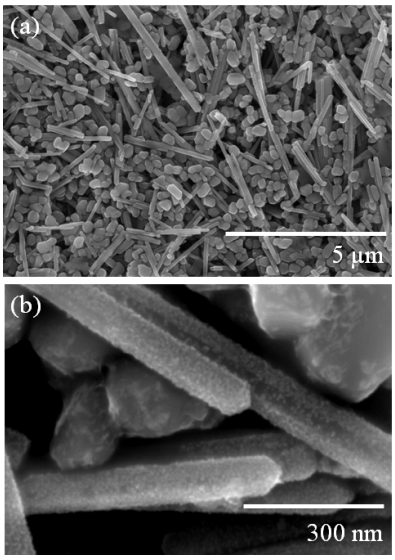

Figure 2. Scanning Electron Microscope images of pressure sensitive ink surfaces: (a) wide view of the ink surface, showing clumps of acicular filler particles and approximately spherical particles dispersed across the surface. Voids in the printed ink are seen across the entire surface. (b) High resolution image of a clump of needles and approximately spherical particles. The approximately spherical particles have a discontinuous surface coating, while the acicular particles are seen to have a rough, nodular surface.

The pressure sensitivity of the electrical resistance is shown as a function of compressive loading in figure 3. Prior to contact with the force probe the resistance typically exceeds 10 MΩ and the resistance exhibits a large reduction even in response to a force as low as 0.1 N. The high initial resistance indicates that there is negligible intimate contact between the lower ink layer and the upper carbon contact until a force is applied to the sensor. The first contact response of the ink to a very low force is observed to occur when there is negligible compression. There is a significant increase in conductivity with less than 0.01 N of force and contact is well established by 0.1 N. This is a consequence of contact established between the upper carbon electrode and the upper surface of the ink principally with the acicular particles that do not lie in the plane of the ink surface. This behaviour contrasts with other highly loaded composites that show little resistive change in response to forces below 5 N.[13,14,22] Typically, the resistance of the test devices falls down towards 10^2 Ω with the application of 3 N of compressive force, a dynamic range highly suitable for many potential applications. The rate at which the resistance changes with applied force decreases as the force increases. Thus, while at negligible force the response is due to an increasingly

intimate contact between the upper carbon and the lower ink, at higher force (>0.1 N) it is due to compression of the ink and a consequent increase in conduction pathways through the ink. Figure 3 also shows the behaviour before and after 1 million cycles of applied force of 10 N, indicating that the loading response of the resistance of the ink is reproducible.

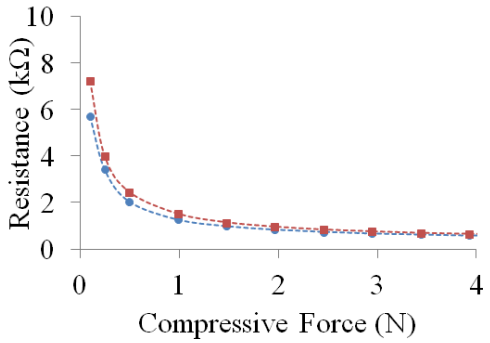

Figure 3. Example data showing the dependence of the electrical resistance on the applied force averaged over five tests for the pressure sensitive ink before (circles) and after (squares) 1 million 10 N dynamic force cycles.

In addition to the force dependence of the resistance, the I-V characteristics of the inks have been subjected to investigation under constant pressure. Applied forces between 0.001 and 10 N were chosen. Some creep behaviour was observable under constant loading with the resistance settling to a constant value in circa ten minutes. Under ten I-V cycles the hysteresis behaviour shows some very subtle variations in the first four or five cycles, but then settles to essentially reproducible behaviour. Examples of the current-voltage behaviour obtained at relatively low and high compressions equating to initial resistances of 52.4 kΩ and 340 Ω respectively are shown in figure 4 (a) and figure 4 (b). At low compression the I-V characteristic is non-linear, with an increasing slope at higher voltages. In contrast at high compression, when the resistance is much smaller, the I-V characteristic is largely linear. The I-V data also reveals some hysteresis between the ramping up and ramping down of the voltage. This is shown more clearly in figure 4 (c) where the resistance is slightly higher when the voltage is ramped down. Under large compressions, the resistance is much lower and the I-V curve is closer to linear, although a small quadratic component is still present. Hysteresis is also present at high compression, but it is reversed at the highest compressions such that the resistance of the ink is slightly lower when the voltage is ramped down, see figure 4 (d). A compression where no hysteresis occurs is therefore possible. Hysteresis has also been observed in a QTC™ nickel-silicone composite, as discussed later.[23]

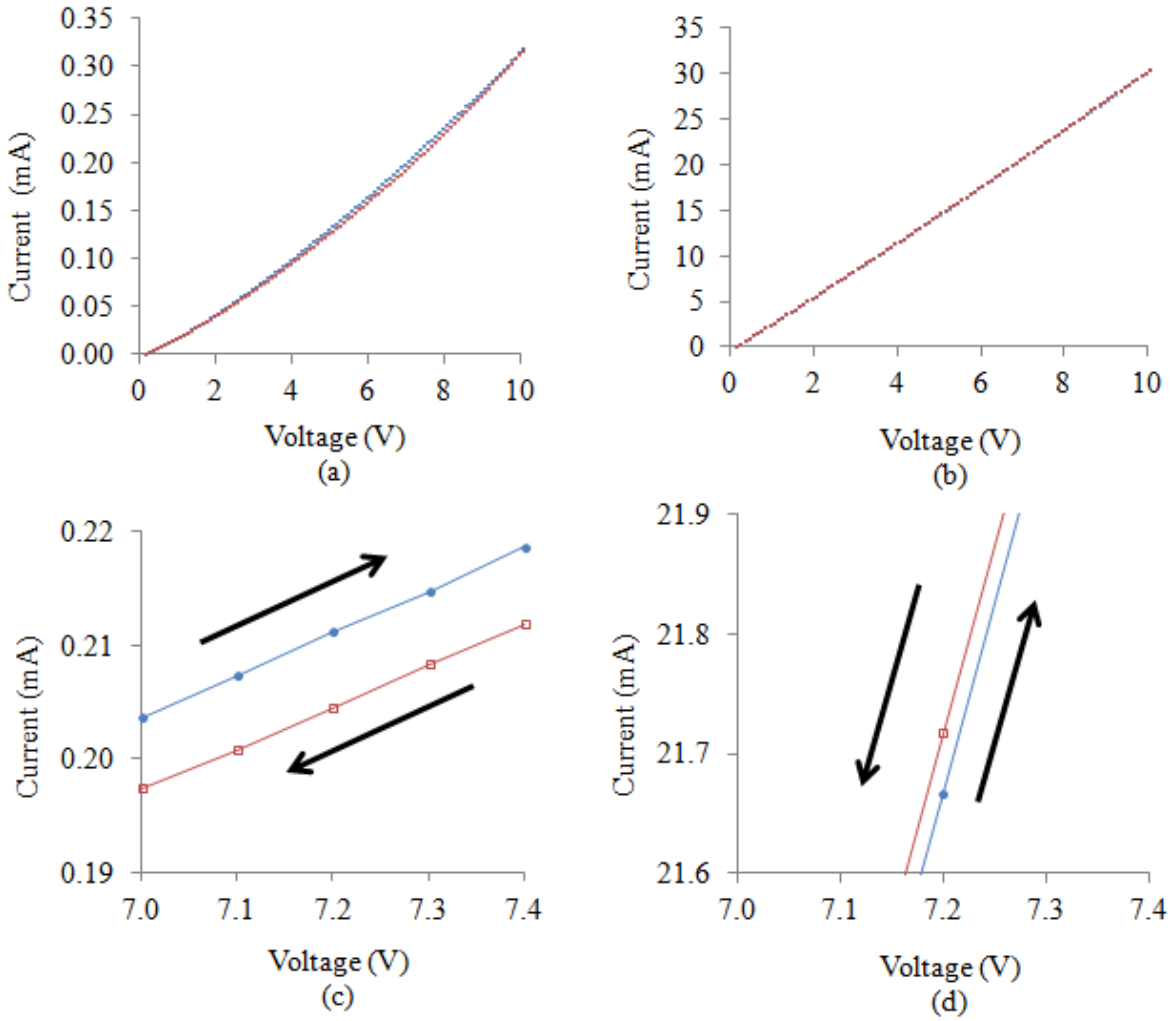

Figure 4. Example of the I-V characteristics of the ink under (a) low and (b) high compression. (c) and (d) respectively show the same I-V data from low and high compressions on an expanded scale to provide a clearer view of the electrical hysteresis. Solid circles indicate data with increasing voltage and the open squares represent data measured with decreasing voltage. Error bars representing the current measurement errors are smaller than the data points.

In order to empirically monitor the change in the I-V behaviour as a function of force, the I-V data was fitted crudely with a combination of linear and quadratic terms of electrical conductance, in accordance with work on random resistor networks (RRN) by Gefen and Chakrabarty, see equation 1.[24,25] This phenomenological model, however, is not based upon any real physical mechanisms and does not provide a detailed insight into electrical conduction processes which may be present in the ink.

$$I = G_1 V + G_2 V^2 \quad (1)$$

Where G_1 and G_2 are respectively the linear and non-linear conductance.

Figure 5 (a) and figure 5 (b) show the variation of the linear and quadratic terms as a function of compressive force. As compression of the ink is increased, both the linear and quadratic conductance increase, however above ~1 N the quadratic conductance begins to fall while the linear component continually rises. Similar non-linear behaviour has also been reported for bulk composites comprising graphite nanosheets and carbon fibres and such behaviour could not be explained by a single conduction mechanism.[26,27] On the basis of prior studies, the most likely explanation for the non-linear I-V behaviour of the ink may arise from some form of field-assisted quantum tunnelling mechanism.[27] The observed I-V behaviour suggests a transition from conduction dominated by complex non-linear conduction mechanism(s) at low compression to more ohmic behaviour at higher compression.

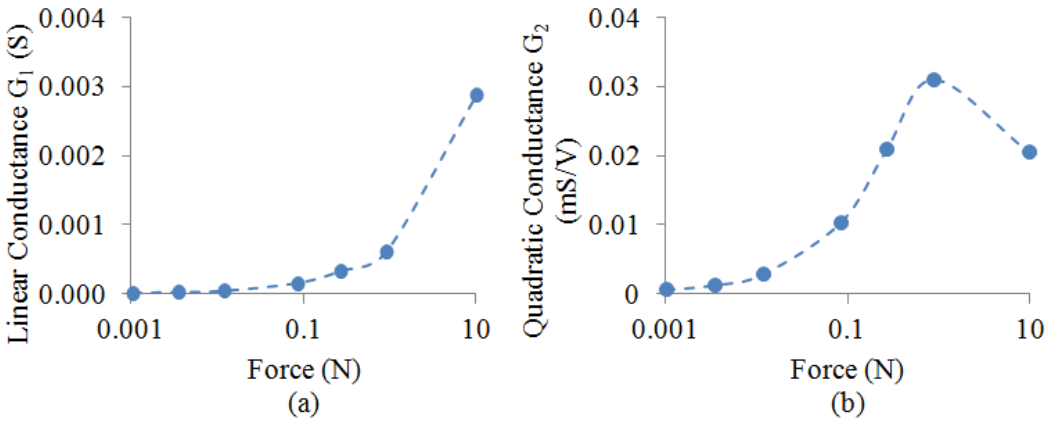

Figure 5. Behaviour of the (a) linear and (b) quadratic conductance terms of the I-V characteristic curves with increasing applied force. Error bars representing the current measurement errors are smaller than the data points.

Various forms of internal field emission exist and their magnitude depends on the strength of the applied electric field across tunnelling barriers.[28,29] These different forms of field assisted tunnelling are shown schematically in figure 6 (a) and figure 6 (b).[27] In the low electric field limit, where the bias across a tunnel barrier is less than the barrier height, charge may flow by direct tunnelling or indirectly via field ionization of impurity states. These are highlighted as (1) and (2) in figure 6 (a). Direct tunnelling is an electrode emission process whereby electrons tunnel from one electrode to the other. In the case of the ink the electrodes are semi-conductor coated nanorods and the insulator is ink residues coated on the nanorods, the less conductive near-spherical particles, or perhaps also air gaps. Field ionization of impurity states is a bulk emission process, involving the tunnelling of electrons from the conduction band of the insulator through to an electrode. It also occurs at higher electric fields. In the high field limit, seen schematically in figure 6 (b), charge transport across the barrier occurs through intra-impurity tunnelling (3), Zener tunnelling (4), electron (5) and hole (6) injection and the aforementioned impurity field ionization. Processes (3) and (4) are bulk emission mechanisms where charge tunnels between impurity states and from the valence to the conduction band of the insulator, respectively. Processes (5) and (6) are analogous to a special form of tunnelling, termed Fowler Nordheim (F-N) field emission.[28] F-N field emission describes the emission of charge through exact or rounded triangular potential barriers at metal-vacuum interfaces and occurs at very high electric fields.

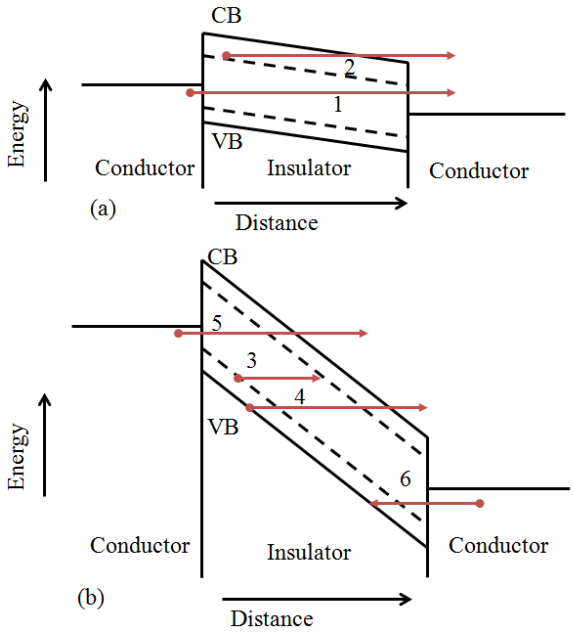

Figure 6. Potential energy diagrams of a metal-insulator-metal junction in the low electric field (a) and high electric field (b) limits. The solid lines labeled VB and CB are the valence and conduction bands of the insulator, respectively, while dashed lines represent impurity states within the forbidden gap of the insulator. The numbered arrows indicate internal field emission processes within the junction: (1) direct (2) field ionization of impurity state (3) intra-impurity (4) zener (5) electron injection and (6) hole injection tunnelling.

He and Tjong (2011 and 2012) describe how internal field emission between isolated clusters of conductive filler particles can be responsible for conduction through a carbon nanofibre/high density polyethylene composite system.[27,30] The total conductivity σ then comprises two contributions; a linear conductivity σ_0 and an internal field emission conductivity σ_{IFE} and the current density $J(E)$ can be represented thus:

$$J(E) = \sigma_0 E + AE^n exp\left(-{}^{B}/_{E}\right) \quad (2)$$

Where E is the applied electric field, A is a function of the tunnelling frequency, B is a measure of the energy barrier and n is an integer that lies between 1 and 3, which depends upon the details of the tunnelling mechanism. The parameter n is equal to 2 in the special case of Fowler-Nordheim (F-N) Tunnelling.[27,31] Figure 7 shows an example of the ink data fitted with this model. The additional exponential field emission term will be most important in the low electric field regime. At high electric fields, equation 2. approximates equation 1. A graphical test of fit using normalized residuals, a measure of the difference between model and observed data, was deemed to be more appropriate than the employment of correlation coefficients or a Chi squared test.[32] A comparison of the normalized residuals in figure 8 from fits of equation 1 and equation 2 to the I-V data reveals that, while still not the complete picture, equation 2 from He and Tjong is a far better fit. In particular, the low field region, circa 1 V in Figure 8, is fitted very well by equation 2, with the residuals very close to zero and in between +/- 2. In comparison, the residuals plot for the RRN model equation 1 show a lot of bias, extending to -10 in the low field region.

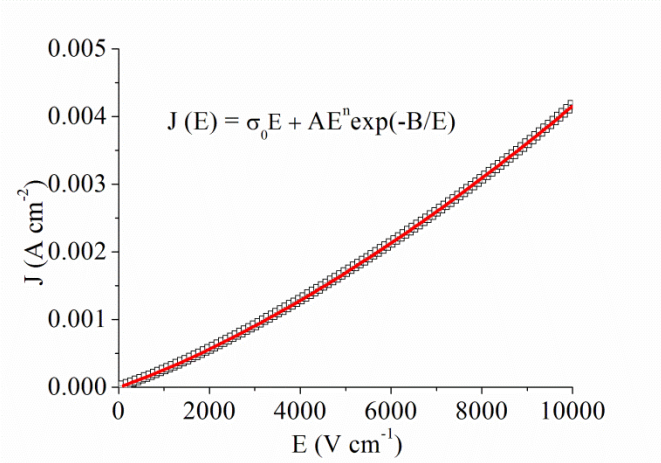

Figure 7. Fitting of equation 2 to experimental data. The red line is the fit, the underlying black squares are the data. Error bars are smaller than the data points.

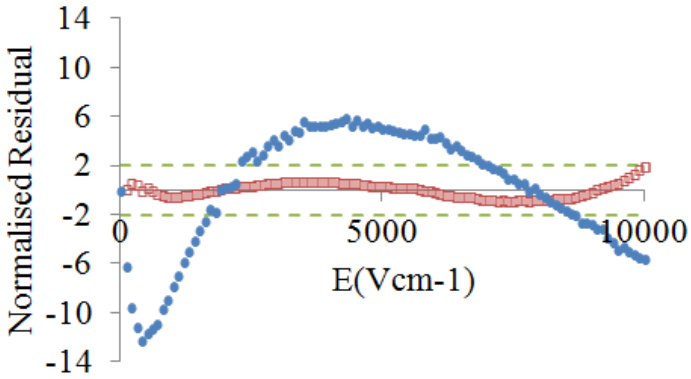

Figure 8. A plot of normalized residuals from fits of random resistor network model equation 1, shown by blue solid circles, and field emission equation 2, shown by red open squares. Dashed green lines at +/- 2 are included as a guide to the eye of the area residuals must lie in for a model fit to be accepted.

Figure 9 (a) and figure 9 (b) show the variation of the linear conductivity σ_0 and the pre-factor A as a function of compressive force (linear scale), while figure 9 (c) and figure 9 (d) show the same variation of linear conductivity and the pre-factor A as a function of compressive force but with a logarithmic scale, respectively. The linear conductivity in figure 9 (a) increases with increasing compression (linear scale), while the declining rate of increase suggests that the linear conductivity is tending towards a maximum value, related to the total number of possible ohmic connections between filler particles/clusters in the composite ink. In figure 9 (b), the parameter A rises with compressive force between 0.1 and 1 N before stalling at ~1 N and falling back to zero. Figure 9 (c) shows there is a dramatic increase in the linear contribution to conductivity which coincides with a dramatic decrease in the non-linear contribution shown in figure 9 (d).

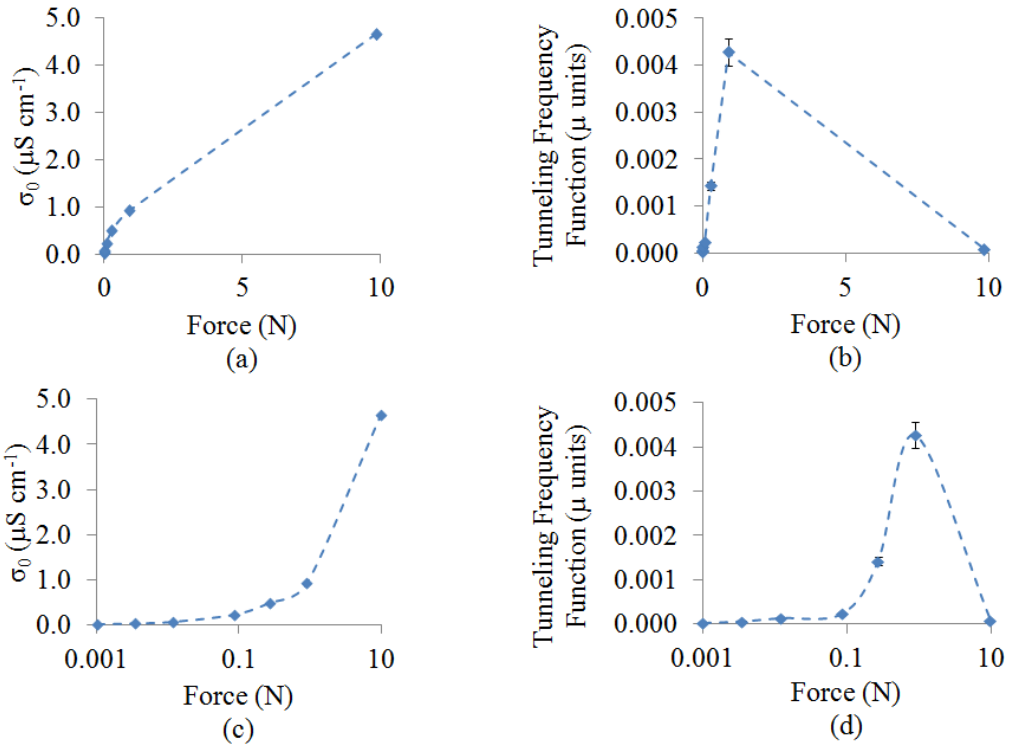

Figure 9. The behaviour of (a) the linear conductivity σ_0 and (b) the function of tunnelling frequency A with applied compressive force (linear scale) from fitting equation 2 to the data. (c) and (d) show the behaviour of linear conductivity and parameter A with compressive force with a logarithmic scale.

This suggests highly sensitive non-linear conduction mechanisms in the low force regime which are lost at high compression, where conductivity is largely ohmic. Unlike the other fitted parameters, the energy barrier parameter, *B*, had a large associated error, often larger than the calculated value. These large errors are likely to signify the presence of a distribution of energy barriers, which may be attributed to local structural variations that are observed in the printed ink. The exponent *n* fluctuated between a value of 1.5 and 2 for inks at all compressions, which may suggest the presence of F-N like tunnelling. To check for F-N tunnelling in the inks, F-N plots, a graph of $\ln(I/V^2)$ against 1/V, of high and low compression I-V cycles are presented in figure 10. F-N plots indicate the presence of F-N tunnelling with a straight, negative gradient line.[33] As figure 10 demonstrates, however, the F-N plots exhibit a positive gradient and non-linear characteristic.

Similar F-N plots have been observed in studies of EuO spin filter tunnel barriers.[34] In this work, a turnover from direct tunnelling to F-N tunnelling was observed at high electric fields. This behaviour would normally suggests F-N tunnelling does not account for the tunnelling conduction in the ink, however one must consider that the I-V curves apply for the bulk material, whereas F-N tunnelling theory was created for describing field emission between parallel electrodes and for single sharp electrodes in vacuum, and so may not be wholly indicative of the presence of F-N mechanisms. The F-N theory also does not account for the combination of internal field emission with the ohmic, percolative conduction mechanisms present in the ink, which would also likely affect exponent *n*. That said, we cannot yet rule out other forms of internal field emission, as described earlier and depicted in figure 6., from contributing to the tunneling conduction in the ink, due in part to the inks complexity.

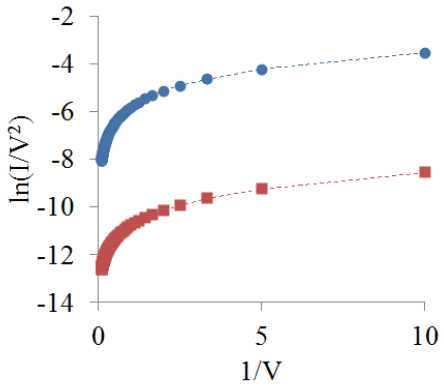

Figure 10. Fowler-Nordheim plots of I-V data from low (red square data points) and high (blue circular data points) compression ink samples.

The behaviour of the parameters σ_0, B and A all indicate that as increasing pressure compresses the ink, the acicular particles move closer together, reducing tunnelling barrier widths which allows greater and more efficient tunnelling current. Contributions to the tunnelling current may include various forms of internal field emission such as direct tunnelling and field ionization of impurity states in the low field limit, and intra-impurity and Zener tunnelling in the high field limit. Ohmic contacts between the acicular particles also form, resulting in an increase of linear ohmic conduction. At ~1 N, further formation of ohmic contacts between acicular particles due to a significant diminution in the size of the aforementioned voids reduces the contribution to conduction from quantum tunnelling mechanisms to such a great extent that linear ohmic connections dominate the conduction. Comparison with figure 3 shows that the different dependencies on force below and above 1 N mirror the change in the sensitivity of the resistance to pressure in the vicinity of 1 N. The structural detail shown in figure 2 together with these factors support the model proposed at the start of this section that the response is determined by carbon-ink contact at < ~0.01 – 0.1 N force and ink compression above this force.

The observed hysteresis in the I-V data suggests that, at low compressions, a higher degree of field assisted quantum tunnelling conduction processes, as compared to linear ohmic percolative conduction, leads to charge becoming trapped at "dangling ends"[35] in the field assisted percolative network. This trapped charge forms potential barriers which act to impede some of the available conduction paths. As noted earlier this effect has been observed in a QTC™ nickel-silicone composite.[23] In this composite internal field emission from the nanoscale features on the surfaces of the nickel particles gives rise to much larger charge trapping. The resulting I-V characteristics are highly non-linear with the resistance falling initially but then becoming very large as trapped charge pinches off the conduction paths. On reversing the voltage sweep large changes in resistance occur as the elastic matrix allows the internal structure of the composite to relax to minimize the total energy. The ink is a much more rigid composite and there will be little internal distortion of the structure due to the trapped charge so that the resistance remains high after the voltage sweep. At higher compressions ohmic conduction through the percolation network dominates, affecting a considerable drop in electrical resistance. The dramatic rise in conductivity results in a 10^2 increase of the current through the ink for a given voltage, which can lead to some joule heating. The ink therefore warms with increasing voltage. As shown in an independent study the ink displays a negative temperature coefficient of resistance, so that the heating results to a slightly lower resistance, which accounts for the reversal of hysteresis behaviour.[36]

The development of conduction by compression induced percolation alongside quantum mechanical tunnelling between particles separated by varying distances has been discussed for model systems of spherical particles.[11] Crossover between these two mechanisms has been characterized by the ratio of the particle diameter to a characteristic tunnelling length. Tunnelling lengths have been deduced for composites containing nanospheres, nanofibres, graphite nanosheets and graphene using model systems comprising uniform ellipsoids with different axial ratios.[37] Values obtained for fibres range from 0.1 to 30

nm. This provides support for the hypothesis that the conduction behaviour of the compressed ink arises from differences in the relative importance of percolative and tunnelling conduction processes. However, direct comparison with the theoretical studies is not possible as the ink which forms the basis of this study has a more complex structure, containing particles of disparate sizes and geometries and thus the occurrence of field assisted tunnelling needs to be taken into account.

4. Conclusions

In summary, a functional ink has been developed that is composed of a combination of semi-conductive acicular and approximately spherical electrically insulating nanoscale particles and displays a very high and reproducible touch pressure sensitivity of its electrical behaviour. These components form a complex structure responsible for the inks' electrical functionality. The specific materials used are not crucial in this regard, only that there is a combination of semi-conductive and insulating particles in an insulating polymer ink, used as a binder and to enable the employment of conventional screen printing technology to create devices. The non-linear I-V characteristics, the small degree of hysteretic electrical behaviour and electron microscopy of the ink surface, which reveals some aggregation of the acicular particles, provide a basis for identifying the likely conduction mechanisms that underlie the touch pressure response. Initially the response of the test structure is determined by changes in the contact between the ink surface and the upper carbon electrode, however once full contact is established the subsequent further reduction in resistance will result from changes in the ink layer as described above. At low compression field assisted tunnelling processes are important and at higher compression direct ohmic connections dominate. The development of this ink presents a unique opportunity for force and position sensing in touchpad technologies.

Acknowledgements

This research was funded and supported by Peratech Ltd. and the EPSRC.

References

1. Shrotriya V 2009 Organic Photovoltaics; Polymer Power. *Nat. Photonics*, **3** 447-499.
2. Chen P, Chen H, Qui J and Zhou C 2010 Inkjet Printing of Single-Walled Carbon Nanotube/RuO2 Nanowire Supercapacitors on Cloth Fabrics and Flexible Substrates. *Nano Res.* **3** 594-603.
3. Lakafosis V, Rida A, Vyas R, Yang L, Nikolaou, S and Tentzeris M 2010 Progress Towards the First Wireless Sensor Networks Consisting of Inkjet-Printed, Paper-Based RFID-Enabled Sensor Tags. *Proc. IEEE*. **98** 1601-1609.
4. Kang J S, Kim H S, Ryu J, Hahn H T, Jang S and Joung J W 2010 Inkjet Printed Electronics Using Copper Nanoparticle Ink. *J. Mater. Sci: Mater. Electron*. **21** 1213-1220.
5. Moon K-J, Lee T-I, Choi J-H, Jeon J, Kang Y-H, Kar J-P, Kang J H, Yun I and Myoung J M 2010 One-Dimensional Semiconductor Nanostructure Based Thin-Film Partial Composite Formed by Transfer Implantation for High-Performance Flexible and Printable Electronics at Low Temperature *ACS Nano*. **5** 159-164.
6. Chang W-Y, Fang T-H, Shen Y-T and Lin Y-C 2009 Flexible Electronics Sensors for Tactile Multiscanning. *Rev. Sci. Instrum.* **80** 084701:1-8.
7. Kim D-K, Kim J-H, Kwon H-J and Kwon Y-H 2010 A Touchpad for Force and Location Sensing. *ETRI J.* **32** 722-728.
8. Norman R. H 1957 *Conductive Rubber*, London: Maclaren.
9. van Beek L. K. H and van Pul B. I. C. F 1962 Internal Field Emission in Carbon Black-Loaded Natural Rubber Vulcanizates. *J.Appl.Polym.Sci.* **6** 651-655.
10. Battacharya S. K and Chaklader A. C. D 1982 Review on Metal-Filled Plastics .1. Electrical-Conductivity. *Polym.Plast.Tech.Eng.* **19** 21-51.

11. Ambrosetti G, Balberg L and Grimaldi, C 2010 Percolation-To-Hopping Crossover in Conductor-Insulator Composites. *Phys.Rev.B.* **82** 134201:1-7.
12. Krivopal B 1999 *U.S. Patent No. 5,989,700*.
13. Knite M, Teteris V, Kiploka A and Kaupuzs J 2004 Polyisoprene-Carbon Black Nanocomposites As Tensile Strain and Pressure Sensor Materials. *Sens. Actuat. A Phys.* **110** 142-149.
14. Qu S and Wong S-C 2007 Piezoresistive Behaviour of Polymer Reinforced by Extended Graphite. *Comp. Sci. Technol.* **67** 231-237.
15. Fujita N, Tojo Y, Matsuba M, Tsuchiyama K, Nishino S, Izaki M and Inoue M 2008 Preparation of Metal-Polymer Composite Films by The Metal-Polymer Co-Electrodeposition Method. *IEEE Trans. Mag.* **44** 2951-2954.
16. Mionić M, Pataky K, Gaal, R, Magrez A, Brugger J and Forró L 2012 Carbon nanotubes-SU8 Composite for Flexible Conductive Inkjet Printable Applications. *J. Mater. Chem.***22** 14030-14034.
17. Lim S, Kang B, Kwak D, Lee W H, Lim J A and Cho K 2012 Ink-Jet Printed Reduced Graphene Oxide/Poly(Vinyl Alcohol) Composite Electrodes for Flexible Transparent Organic Field-Effect Transistors *J. Phys. Chem. C.* **116** 7520-7525
18. Loffredo F, De Girolamo Del Mauro A, Burrasca G, La Ferrara V, Quercia L, Massera E, Di Francia G and Della Sala D 2009 Ink-Jet Printing Technique in Polymer/Carbon Black Sensing Device Fabrication. *Sensors and Actuators B.* **143** 421-429.
19. De Girolamo Del Mauro A, Grimaldi I A, Loffredo F, Massera E, Polichetti T, Villani F and Di Francia G 2010 Improvement of the Inkjet Printed VOCs Sensor Performances Through The Sensing Layer Geometry. *AIP Conf. Proc.* **1255** 345-347.
20. Hsieh G-W, Li F M, Beecher P, Nathan A and Wu Y 2009 High Performance Nanocomposite Thin Film Transistors with Bilayer Carbon Nanotube-Polythiophene Active Channel by Ink-Jet Printing. *J. Appl. Phys.* **106** 123706:1-7.
21. Peratech Ltd., *UK Patent GB 2462920*
22. Abyaneh M K and Kulkarni S K 2008 Giant Piezoresistive Response in Zinc-Polydimethylsiloxane Composites Under Uniaxial Pressure. *J.Phys.D:Appl.Phys.* **41** 135405:1-7.
23. Bloor D, Donnelly K, Hands P J, Laughlin P and Lussey D 2005 A Metal-Polymer Composite with Unusual Properties. *J.Phys.D:Appl.Phys.* **38** 2851-2860.
24. Gefen Y, Shih W H, Laibowitz R B and Viggiano J M 1986 Nonlinear Behaviour Near the Percolation Metal-Insulator Transition. *Phys. Rev. Lett.* **57** 3097-3100.
25. Chakrabarty R K, Bardhan K K and Basu A 1991 Nonlinear I-V Characteristics Near the Percolation Threshold. *Phys. Rev. B.* **44** 6773-6779.
26. Lin H, Lu W and Chen G 2007 Nonlinear DC Conduction Behaviour in Epoxy Resin/Graphite Nanosheets Composites. *Physica B*. **400** 229-236.
27. He L and Tjong S-C 2011 Nonlinear Electrical Conduction in Percolating Systems Induced by Internal Field Emission. *Synth. Metals*. **161** 540-543.
28. Duke C. B 1969 *Tunnelling in Solids*, Academic Press.
29. Chynoweth A G 1960 *Progress in Semiconductors*, J. Wiley **4** 95.
30. He L and Tjong S-C 2012 Universality of Zener Tunneling in Carbon/Polymer Composites. *Synth. Metals*. **161** 2647-2650.
31. Fowler R H and Nordheim L 1928 Electron Emission in Intense Electric Fields. *Proc. R. Soc. Lond. A*. 173-181
32. Hughes I G and Hase T P A 2010 *Measurements and their Uncertainties*, 1st Ed. Oxford.
33. Stern T E, Gossling B S and Fowler R H 1929 Further Studies in the Emission Of Electrons from Cold Metals. *Proc. R. Soc. Lond. A,* **124** 699-723.
34. Müller M, Miao G-X and Moodera J-S 2009 Exchange Splitting and Bias Dependent Transport in EuO Spin Filter Tunnel Barriers. *EPL*. **88** 47006:1-5.
35. Moukarzel C and Duxbery P M 1999 Comparison of Rigidity and Connectivity Percolation in Two Dimensions. *Phys. Rev. E.* **59** 2614-2622.

36. Simon D 2012 *Private Communication*.
37. Ambrosetti G, Grimaldi C, Balberg L, Maeder T, Danani A and Ryser P 2010 Solution of the Tunnelling-Percolation Problem in the Nanocomposite Regime. *Phys.Rev.B.* **81** 155434:1-23.